Ocean Dynamics (2017) 67:383–396
DOI 10.1007/s10236-017-1045-4

A study case of bioluminescence potential dynamics in the Delaware Bay with observations and modeling

Igor Shulman[1] · Mark A. Moline[2] · Stephanie Anderson[1] · Peter Sakalaukus[1] · Clark Rowley[1] · Sherwin Ladner[1]

Received: 6 September 2016 / Accepted: 3 March 2017 / Published online: 17 March 2017

Abstract Results from first observational program of bioluminescence (BL) potential in the Delaware Bay area are presented. During the field program July 30–August 1, 2015, the satellite Visible Infrared Imaging Radiometer Suite (VIIRS) imagery shows the development of the submesoscale filament with elevated chlorophyll-a in the area of interaction of lighter water masses of the Bay outflow with denser upwelled water. We have shown that ageostrophic secondary circulation (ASC) cells contributed to the development of this filament. Analysis of BL potential observations have shown elevated values of BL potential in the area of the submesoscale filament. Analysis of observed temperature, salinity, sigma-t, and BL potential along the stations crossing the Bay mouth have shown a presence of a strong frontal structure separating colder, more saline, denser offshore water from the bay water masses. Over 3 days of sampling, this frontal structure moved onshore to the entrance of the bay, and brought offshore BL plankton communities with higher values of BL potential. We compared two surveys (at the end of July and in the middle of August) of water masses located in the area where the buoyant outflow of the Delaware Coastal Current is turned around and taken to the north up the shelf by upwelling favorable winds. Analysis of observations shows that the survey at the end of July has fresher water masses (due to higher river runoff before and during survey) and higher values of BL potential in comparison to the survey at the middle of August.

Keywords Coastal processes · Upwelling · Submesoscale processes · Bioluminescence · River outflow · Numerical modeling

Responsible Editor: Alejandro Orfila

✉ Igor Shulman
igor.shulman@nrlssc.navy.mil

[1] Oceanography Division, US Naval Research Laboratory, Stennis Space Center, Hancock County, MS 39529, USA

[2] School of Marine Science and Policy, University of Delaware, Lewes, DE, USA

1 Introduction

Bioluminescence (BL) is a light produced by a photochemical reaction in organisms. The major groups of marine organism known to be bioluminescent are bacteria, dinoflagellates, radiolarians, cnidarians, ctenophores, cephalopods, ostracods, copepods, euphausiids, decapod shrimps, and fishes (Haddock et al. 2010; Widder 2010; Moline et al. 2013). Most bioluminescent organisms in the marine environment generate light in response to mechanical stimulation, like in the wakes of moving ships or other bodies. BL potential is defined as the flash potential measured inside of a chambered pump-through bathyphotometer (Herren et al. 2005; Moline et al. 2005), which mechanically stimulates organisms to produce light as seawater is pumped through a detection chamber.

Recent reviews of observational and modeling studies of BL potential can be found in (Haddock et al. 2010; Moline et al. 2013; Marcinko et al. 2013). The model of BL potential based on empirical relationships between BL potential and other biogeochemical environmental variables such as chlorophyll was proposed in Ondercin et al. (1995). Seasonal patterns in BL potential by explicitly modeling the population dynamics of bioluminescent dinoflagellates within the North Atlantic region were presented in Marcinko et al. (2014). In our

previous research in the Monterey Bay area, we have shown that dynamics and changes of BL potential are controlled by the interaction of physical processes (upwelling/downwelling, advection, submesoscale dynamics) with biochemical processes, as for example the growth and accumulation of bioluminescent motile species in convergence zones (Moline et al. 2009, 2013; Shulman et al. 2011, 2012, 2015). Our modeling efforts were focused on evaluating the short-term (1–3 days) predictions of the BL potential. Combining dynamical, predictive physical, biochemical, and bioluminescence intensity models, we were able to produce one of the first pictures of BL potential for the Monterey Bay region (Shulman et al. 2011).

In the present paper, we present the first (to our knowledge) observational and modeling studies of BL potential dynamics in the Delaware Bay area to evaluate BL potential at the interface of an estuary-shelf system. Among the species observed in the Delaware Bay area and known to produce light are dinoflagellates, centropages, copepods, amphipods, caldocerans, shrimp, larvaceans, and stenophores (J. Cohen, personal communications).

The variability of atmospheric forcing and interaction with river runoff and tides are major contributors to the dynamics of physical and bio-optical properties in the Delaware Bay (Pennock and Sharp 1986; Sanders and Garvine 2001; Fong and Geyer 2001; Houghton et al. 2004; Whitney and Garvine 2005, 2006; Muscarella et al. 2011; Wang et al. 2012; Joesoef et al. 2015). The greatest amount of the river discharge in the area occurs during the spring months due to snow melt and spring rains (Sanders and Garvine 2001). Downwelling favorable winds tend to accelerate downshelf flow of the river outflow to the south, while upwelling favorable winds counter the buoyancy-driven downshelf flow and take buoyant waters offshore and up the shelf to the north (Whitney and Garvine 2005, 2006).

We conducted BL potential surveys during 2–3 consecutive nights in June–August of 2015. It is clear that 2–3-day durations of ship surveys do not provide enough spatial and temporal coverage to establish relations between physical, bio-optical processes and BL potential dynamics in the Delaware Bay. The objectives of this study were to describe the first ever survey of the BL potential in the area, to provide the first ever quantitative and qualitative information on the status of BL potential changes in the area, to investigate the sustained BL potential sampling time at a particular depth, and to relate (when possible) the BL potential observations and dynamics to the satellite-observed phytoplankton filaments and corresponding atmospheric conditions.

The paper is organized as follows: Section 2 describes methods which include observations, models used in this study, and investigation of the optimal duration of BL potential sampling at a particular depth. Results are presented in Section 3. Section 4 is devoted to discussions and conclusions.

2 Methods

2.1 Observations

Ship surveys of BL potential were conducted using the Underwater Bioluminescence Assessment Tool (UBAT; WetLabs, Inc., Philomath, OR) at set stations shown on Fig. 1. The UBAT temporal resolution is 60 Hz (60 samples per second). During downcast surveys, BL potential was sampled at specific depths (1, 6, 11, and sometime at 16 m) for extended periods, while the upcasts were done at a continuous rate (Fig. 1, see also Section 2.3). In addition to the UBAT, the ship profiler was equipped with SBE 37 CTD (SeaBird Electronics Inc., Bellevue, WA).

Surface current observations were downloaded from the Mid-Atlantic Regional Association Coastal Ocean Observing System (MARACOOS). Surface currents are derived from a network of SeaSonde-type Coastal Ocean Dynamics Applications Radars (CODAR) instruments deployed in the Delaware Bay region. SeaSonde-type HF radar instruments exploit information in the radiowave backscatter from the ocean surface to infer movement of the near surface water. Surface currents derived from the Delaware Bay HF radar network validated in Muscarella et al. (2011).

Wind velocity data for the NOAA station at Lewes, DE (Fig. 1), were downloaded from the NOAA station website:
http://tidesandcurrents.noaa.gov/stationhome.html?id=8557380#obs

Level-1B imagery from the Suomi National Polar-orbiting Partnership (SNPP) Visible Infrared Imaging Radiometer Suite (VIIRS) was processed to levels 2 (sensor grid), 3 (mapped grid), and 4 (composites) using the Naval Research Lab's Automated Processing System (APS) (http://www7333.nrlssc.navy.mil/docs/aps_v6.4/html/user/aps.xhtml). APS estimates chlorophyll-a by the OCI algorithm (Hu et al. 2012) at 0.75-km pixel resolution. Numerous validation studies of VIIRS imagery against in situ observations were conducted along the east coast of USA (Arnone et al. 2012; Ladner et al. 2014).The diffuse attenuation coefficient Kd (488) was estimated in accordance with (Lee et al. 2005). The Kd (488) was used to estimate the euphotic depth (noted Eu); the Eu was estimated as the depth where photosynthetic available radiation (PAR) is 1% of its surface value (Lee et al. 2007):

$$\mathrm{Eu} = -\ln(0.01) \Big/ \mathrm{Kd}(488)$$

2.2 Models

The fine-resolution model around the Delaware Bay (named FDEL) is based on the Navy Coastal Ocean Model (NCOM), which is a primitive-equation, 3D, hydrostatic model. It uses the Mellor-Yamada level 2.5 turbulence closure scheme, and

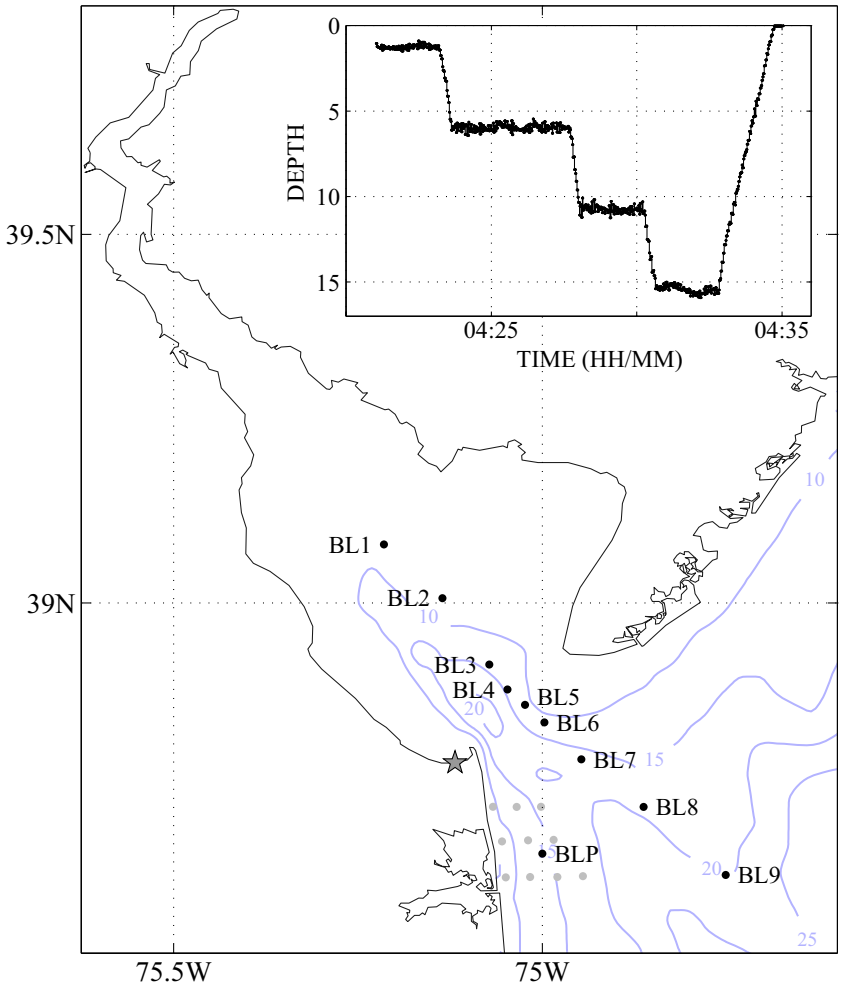

Fig. 1 The locations of stations sampled during the nights of June 12 and July 30–August 1, 2015 (shown by *dark dots*) and August 19, 2015 (shown by *gray dots*); the location of the NOAA station at Lewes, DE (*star*), contours of bathymetry and plot of the downcast and upcast profiles sampled at station BL8 during the night of June 12

the Smagorinsky formulation for horizontal mixing. The FDEL model is set up with 0.5-km horizontal resolution, and the model domain extends to 73.36 W offshore and from 37.96 N to 39.8 N (Fig. 1). Open boundary conditions for the FDEL model are derived from the coarser resolution (3 km) and larger domain regional model (CDEL) which extends offshore to 72.77 W and from 37.4 N to 40.4 N. Open boundary conditions for the CDEL model are derived from the HYCOM global model, which has 1/12° horizontal resolution (Chassignet et al. 2009; Metzger et al. 2014). The tidal forcing for the CDEL model is applied by superimposing tidal elevation and transport for eight tidal constituents (K1, O1, P1, Q1, K2, M2, N2, and S2) on the (non-tidal) boundary data from the global HYCOM using a Flather open boundary condition (Flather 1976). The tidal data are from the OSU global tidal database (Egbert and Erofeeva 2002). Both FDEL and CDEL models are forced with surface fluxes from the Coupled Ocean and Atmospheric Mesoscale Prediction System of the North West Atlantic (COAMPS_NWATL). According to Sanders and Garvine (2001), the US Geological Survey (USGS) Delaware River discharge record at Trenton, NJ, provides a good measure of river outflow and it is proportional to outflow at the bay mouth. The USGS daily river discharge record at Trenton, NJ, is used to simulate river inflow in the models. The FDEL and CDEL models use the Navy Coupled Ocean Data Assimilation (NCODA) system (Cummings 2005) for the assimilation of available satellite-derived SST and SSH data, as well as available in situ temperature and salinity observations from the NAVOCEANO data streams. In this study, a depth of mixed layer (MLD) is derived from the FDEL model. The MLD is computed as the depth at which temperature deviates by 0.3 °C from the temperature at the near surface at 2-m depth (Kara et al. 2003).

2.3 Investigation of sustained BL potential sampling time at a particular depth.

During the first survey (Fig. 1, night of June 12, 2015) we investigated the optimal duration of BL potential sampling at a particular depth in order to account for the variability in organisms' abundance. We considered all possible sub-segments of 0.5-min duration from ~3-min segment taken at 6-m depth at station BL8 (Fig. 1), each of the possible 0.5-min sub-segments was numbered and for each of possible 0.5-min

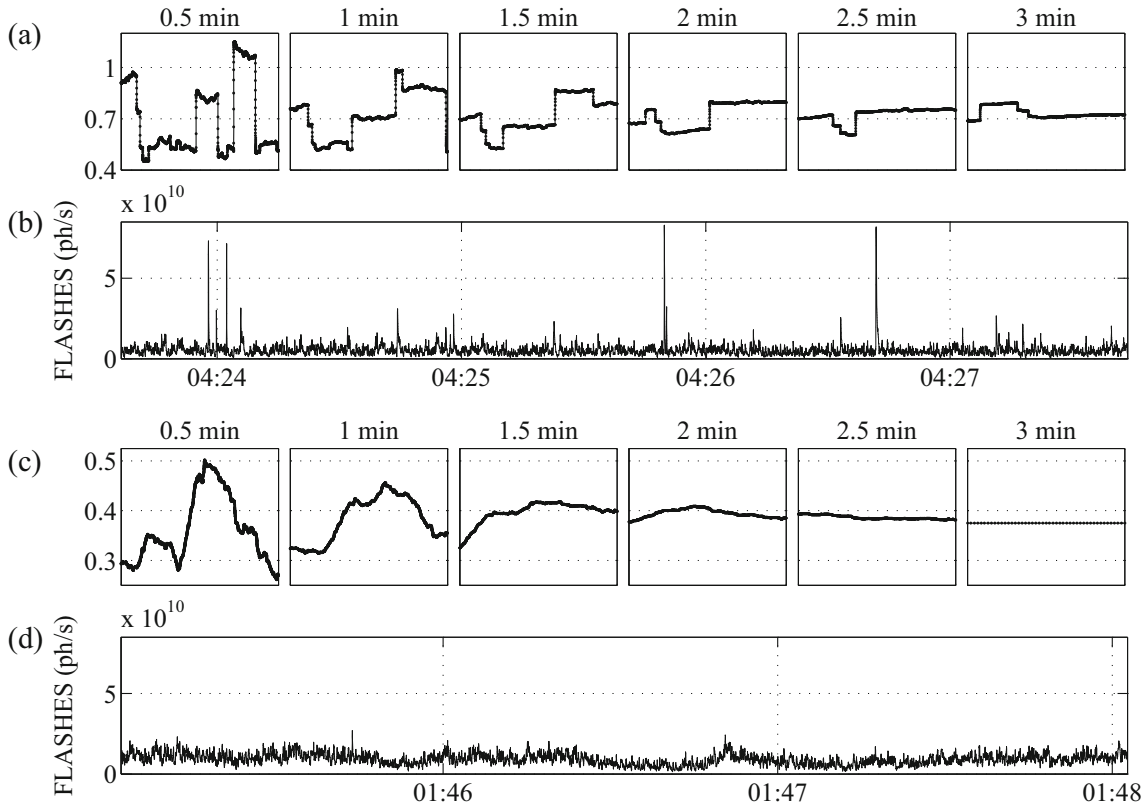

Fig. 2 **a** Estimated ratios of the std/mean as a function of the sub-segment number for 0.5-, 1-, 1.5-, 2-, and 2.5-min possible segments for station BL8 at 6-m depth. **b** BL potential flashes at 6-m depth for station BL8. **c** Estimated ratios of the std/mean as a function of the sub-segment number for 0.5-, 1-, 1.5-, 2-, and 2.5-min possible segments for station BL2 at 1-m depth. **d** BL potential flashes at 1-m depth for station BL2

sub-segment, we estimated the ratio of standard deviation (std) of observed BL potential to the mean of BL potential. Then, we performed the same statistics for each possible 1-, 1.5-, 2-, and 2.5-min sub-segments. Figure 2a shows plots of estimated ratios of the std /mean as a function of the sub-segment number. It shows that sampling with duration around 2 to 2.5 min is flattening the ratio of standard deviation to the mean of the BL potential. Deviation from the flattening is determined by a few high-intensity flashes (Fig. 2b) which are likely associated with bioluminescent jellies (Widder and Johnsen 2000; Moline et al. 2010; Johnsen et al. 2014; Cronin et al. 2016). The same analysis was conducted for the station BL2 (Fig. 1) which is located inside the bay. As for station BL8, Fig. 2c also shows the flattening of the ratio of standard deviation to the mean for the duration of sampling at a particular depth around 2 to 2.5 min. BL potential flashes for the BL2 at 1 m (Fig. 2d) are more uniform than BL potential flashes for the station BL8 at 6 m (Fig. 2b). This explains why the ratio of standard deviation to the mean is more flattened for sampling from 2- to 2.5-min duration in case of station BL2 in comparison to the station BL8. Based on the described analysis, we stayed within 2 to 2.5 min at each depth during downcasts for other surveys conducted during July–August of 2015.

3 Results

During the field program of July 30–August 1, 2015, stations shown on Fig. 1 were sampled for three consecutive nights to study temporal and spatial variability in BL potential. These are the same stations sampled during the night of June 12 plus stations BL1 deeper inside the bay, the more offshore station BL9, and a station called "BLP" indicating the location of the station in the area of the buoyant Delaware Bay outflow. Hourly averaged 10-m wind velocities from the NOAA station at Lewes, DE, are shown in Fig. 3. During three consecutive nights of sampling, there were upwelling favorable winds, with somewhat weaker winds during the night of July 31, and there was a short reversal of winds between nights of July 31 and August 1. Figure 3 also shows 10-m wind velocities from the atmospheric model COAMPS_NWATL (used to force the FDEL model, see Section 2.2) at the NOAA Lewes, DE, station location. We estimated the magnitude of the complex correlation coefficient and angular displacement (Kundu 1976; Shulman et al. 2010) between observed and COAMPS_NWATL model 10-m wind velocities presented on Fig. 3. The complex correlation between observed and model wind velocities is estimated over 4 days using hourly data. In this case, the correlation

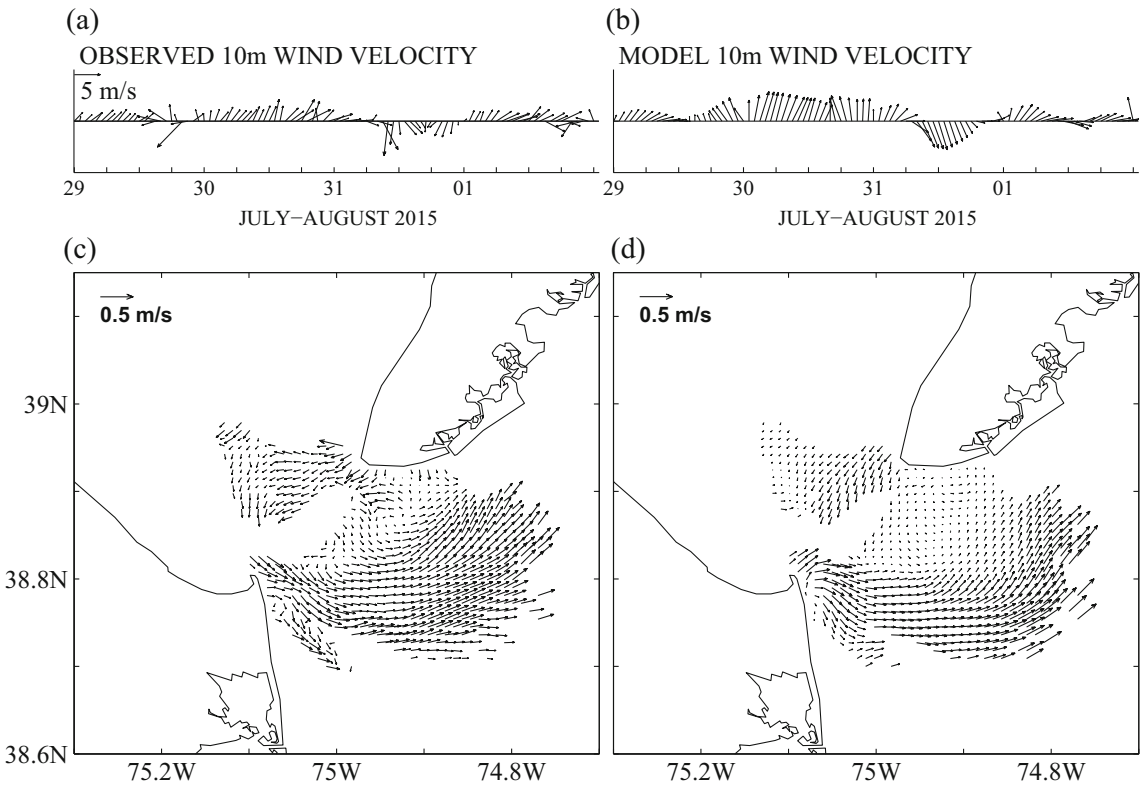

Fig. 3 **a** Ten-meter wind velocities at the NOAA station at Lewes, DE, and **b** from the atmospheric model COAMPS_NWATL (used to force the oceanic model FDEL), **c** 33-h low-pass filtered HF radar, and **d** the FDEL surface currents on July 31, 2015

around 0.2 is considered as significant at a 95% confidence level for the number of degrees of freedom around 96 (see, e.g., Wilks 1995). The estimated value of complex correlation between observed and model wind velocities is 0.55, which is significant at a 95% confidence level. The angular displacement between model and observed wind velocities is small and equals −9.64°. Figure 3 also shows reasonably good agreement in magnitudes and directions between the HF radar and FDEL model surface currents (currents are 33 h low-pass filtered), which is probably a result of significant correlation and small angular displacement in the observed and COAMPS predicted 10-m wind velocities. HF radar and model surface currents show typical surface circulation patterns as observed previously during the upwelling events in the Delaware Bay (Whitney and Garvine 2005, 2006; Muscarella et al. 2011). It is known that a buoyant outflow through the south of the Delaware Bay mouth is transported up the shelf by northward currents during the upwelling favorable winds (Whitney and Garvine 2006).

Figure 4 shows the FDEL model sea surface temperature (a) and sea surface salinity (b) on 00Z of July 31, 2015. There is a fresher water outflow through the southern portion of the Delaware Bay mouth. This less-saline water mixes with cold, more saline upwelled offshore water. The satellite VIIRS image (Fig. 4c) indicates development of the filament with elevated chlorophyll-a content. Because of a predominantly northward flow during the upwelling (Fig. 3), we can suspect that the advection of the Delaware Bay outflow with relatively high chlorophyll water masses contributed to the development of the filament in Fig. 4c. At the same time, Figs. 4a–c show that the filament is maintained in the frontal area of interaction of lighter water masses of the outflow with denser upwelled water. Due to this interaction, the surface frontogenesis develops (Hoskins 1982; Calil and Richards 2010; Levy et al. 2012; Shulman et al. 2015), which leads to an ageostrophic secondary circulation (ASC). These ASC cells are generated in a plane perpendicular to the density front (Hoskins 1982), which are upward (upwelling) on the light side of the front and downward on the dense side of the front. In such regions, the Rossby number is O(1), and the ASC cells lead to a restratification flow from the light side to the dense. This is well-illustrated in Figs. 4d–g, which show the model subsurface profiles of the temperature, salinity, vertical (w), and meridional (v) velocities at 00Z of July 31 along the meridional section noted AA at longitude 74.9 W. There is the development of the ASC cell, with the ascending part of this cell coinciding with the warm, fresher part of the front, and descending part of this cell coinciding with the colder, more saline part of the front. Profiles of w (Fig. 4f) and v (Fig. 4g) show: mostly northward and toward the front flow in the horizontal direction (v is positive, which is typical during upwelling) and with the upwelling flow (w is positive) on the warm

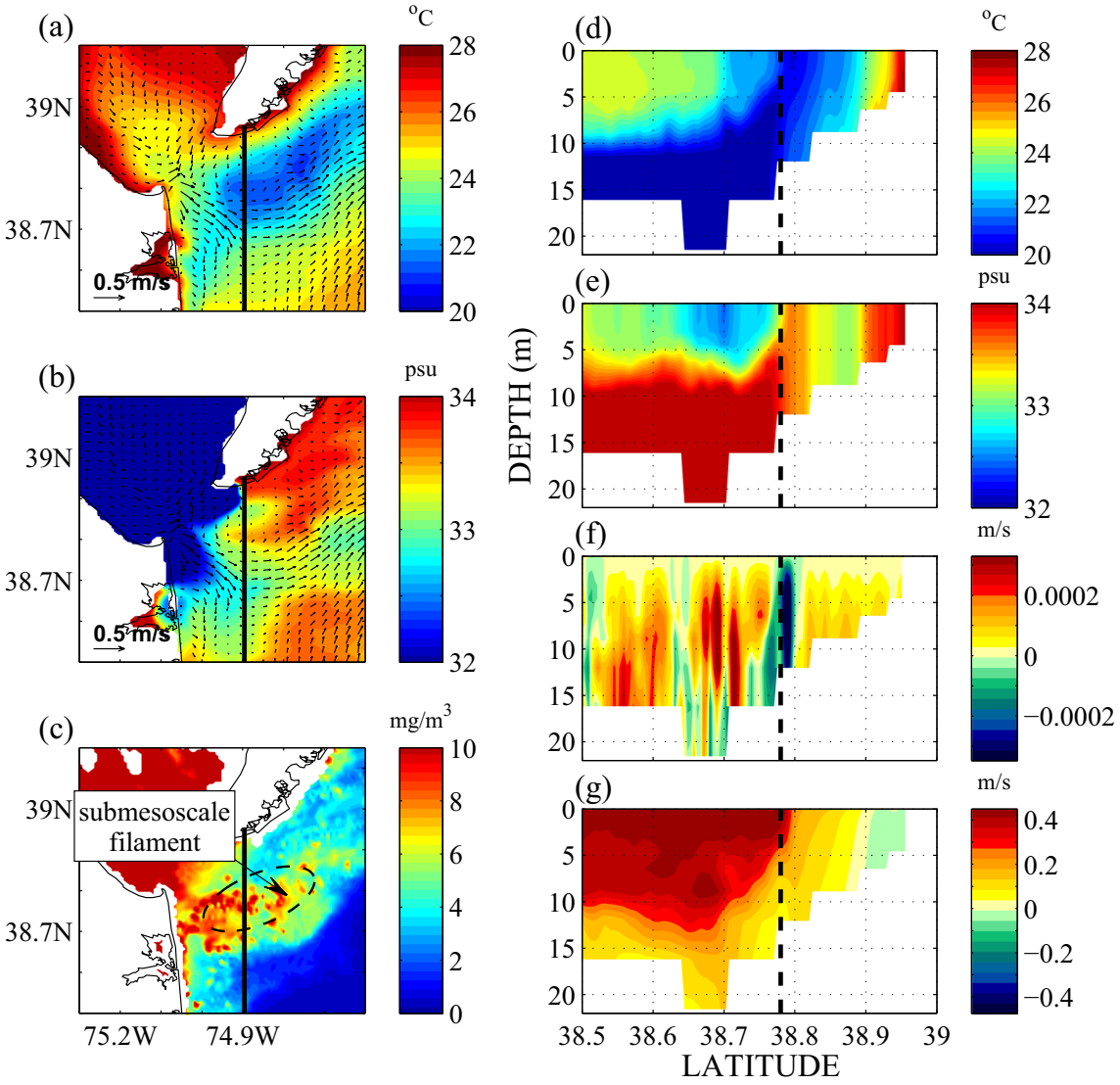

Fig. 4 **a** The FDEL model sea surface temperature and **b** sea surface salinity on 00Z of July 31 of 2015. **c** The satellite VIIRS image on July 31, 2015, location of submesoscale filament with elevated chlorophyll-a content is emphasized with dashed ellipse. **d** The FDEL model subsurface temperature, **e** salinity, **f** vertical velocity, and **g** meridional velocity along meridional section AA (shown on images **a**–**c**) at 74.9 W on 00Z of July 31, 2015

side of the front (in accord with ASC cells). There is the much weaker northward and away from the front horizontal flow and downwelling (w is negative) on the dense side of the front (again in accord with ASC cells). The model results are in agreement with what would be expected from the surface frontogenesis (Hoskins 1982) and with subsurface circulation patterns and mixing reported in previous studies of the Delaware Bay outflow dynamics during upwelling favorable winds (Houghton et al. 2004; Fong and Geyer 2001).

In Hoskins (1982), the Q vector is used to qualitatively diagnose ageostrophic vertical motion due to frontogenesis:

$$Q = \left(-\frac{\partial u_g}{\partial x}\frac{\partial b}{\partial x} - \frac{\partial v_g}{\partial x}\frac{\partial b}{\partial y}, -\frac{\partial u_g}{\partial y}\frac{\partial b}{\partial x} - \frac{\partial v_g}{\partial y}\frac{\partial b}{\partial y} \right) \quad (1)$$

where u_g and v_g are the horizontal geostrophic velocities, and $\frac{\partial b}{\partial x}$ and $\frac{\partial b}{\partial y}$ are the horizontal gradients of buoyancy:

$$b = -g\frac{\rho^*}{\rho_0} \quad (2)$$

with ρ^*being the deviation from the reference density ρ_0, and g is the acceleration due to gravity. The local maximum of Q creates a vertical circulation with associated upwelling/downwelling ASC cells. In the present study, we use the magnitude of the vector Q estimated from the model outputs as an indicator where strong vertical motion and ASC cells might occur. Note that the vector Q has been used to estimate corresponding vertical motions (see for example, Rudnick 1996;

Pollard and Regier 1992), which is not needed in our case because the circulation model gives us vertical velocity directly.

It is known (Calil and Richards 2010; Levy et al. 2012; Shulman et al. 2015) that ASC cells impact phytoplankton growth and increase productivity in a variety of ways, as for example, by modulating the vertical supply of nutrients into the euphotic, lighted layer, or by changing the light exposure of phytoplankton by modulating the strength of vertical mixing.

Figure 5 shows observed and modeled-predicted properties plotted along the meridional section AA crossing the submesoscale filament at longitude 74.9 W. The vector Q magnitude (1) and the mixed layer depth (MLD) were estimated by using the FDEL model fields of temperature, salinity, and velocity averaged over a period of 48 h centered on 00Z of July 31, 2015. Estimated values of Q were also averaged over the top 5-m depth. Location of the local maximum of Q (1) coincides with the location of the chlorophyll filament (Fig. 5) which indicates presence of ASC cells in the area of the filament. Also, the MLD estimated from the FDEL (see the end of Section 2.2) is around 7–10 m, and it is shallower than the estimated euphotic depth (Eu, see Section 2.1) in and around the filament (Fig. 5). In this case, the developed ASC cells kept phytoplankton in the lighted area and supported photosynthesis and phytoplankton growth. The filament is formed during the upwelling, and the ASC cells support a vertical supply of nutrients into the euphotic

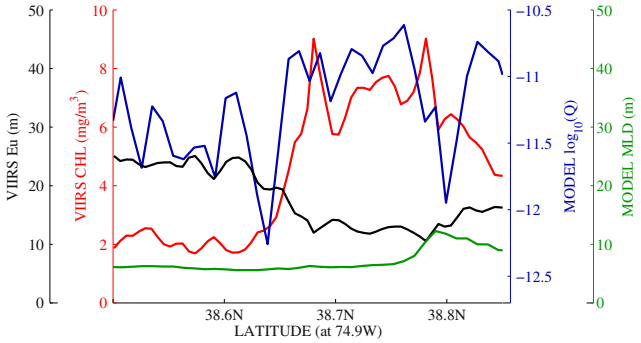

Fig. 5 Observed and modeled-predicted properties plotted along the meridional section AA crossing the submesoscale filament on Fig. 4c: *red* VIIRS chlorophyll-a; *blue* magnitude of the Q vector, *black* euphotic depth, *green* mixed layer depth (MLD)

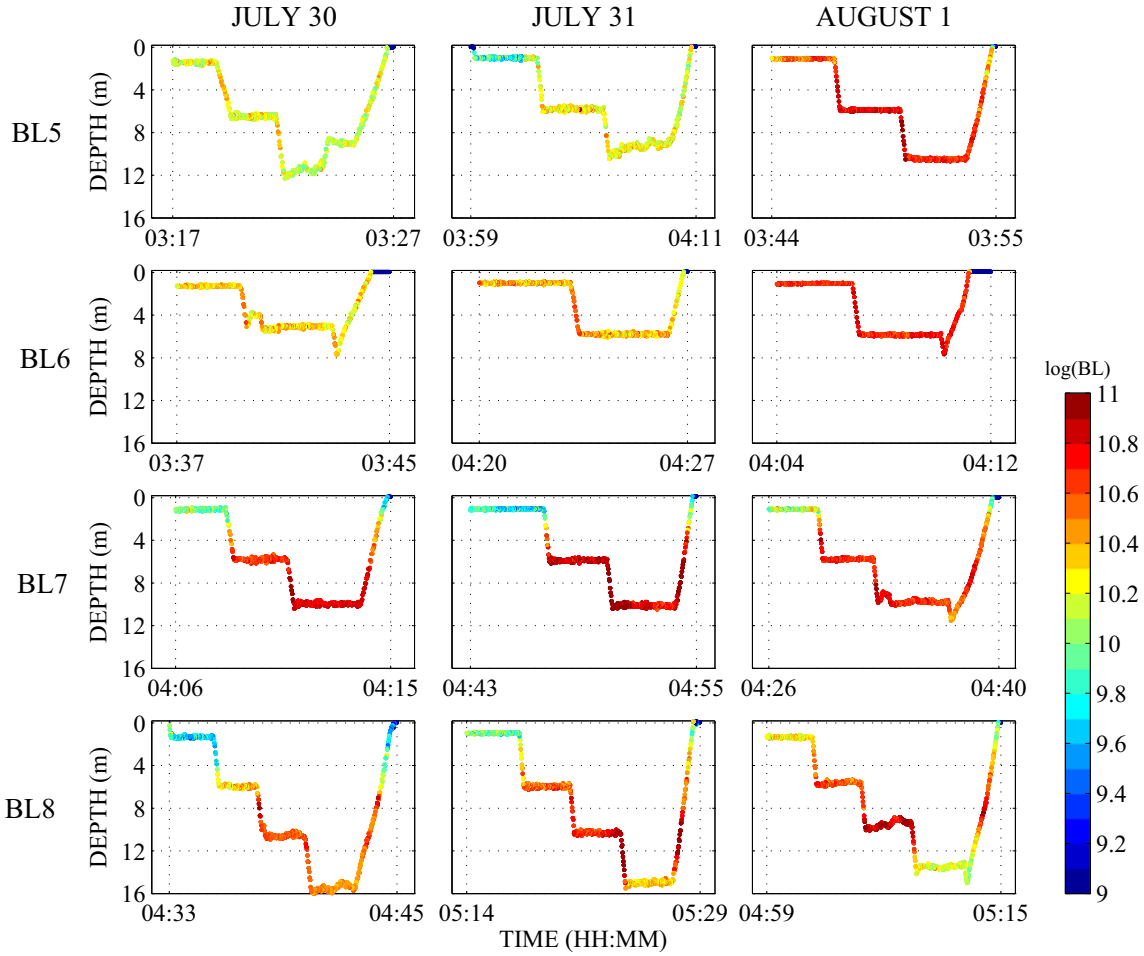

Fig. 6 Observed profiles of the BL potential over 3 days of sampling at stations BL5, BL6, BL7, and BL8

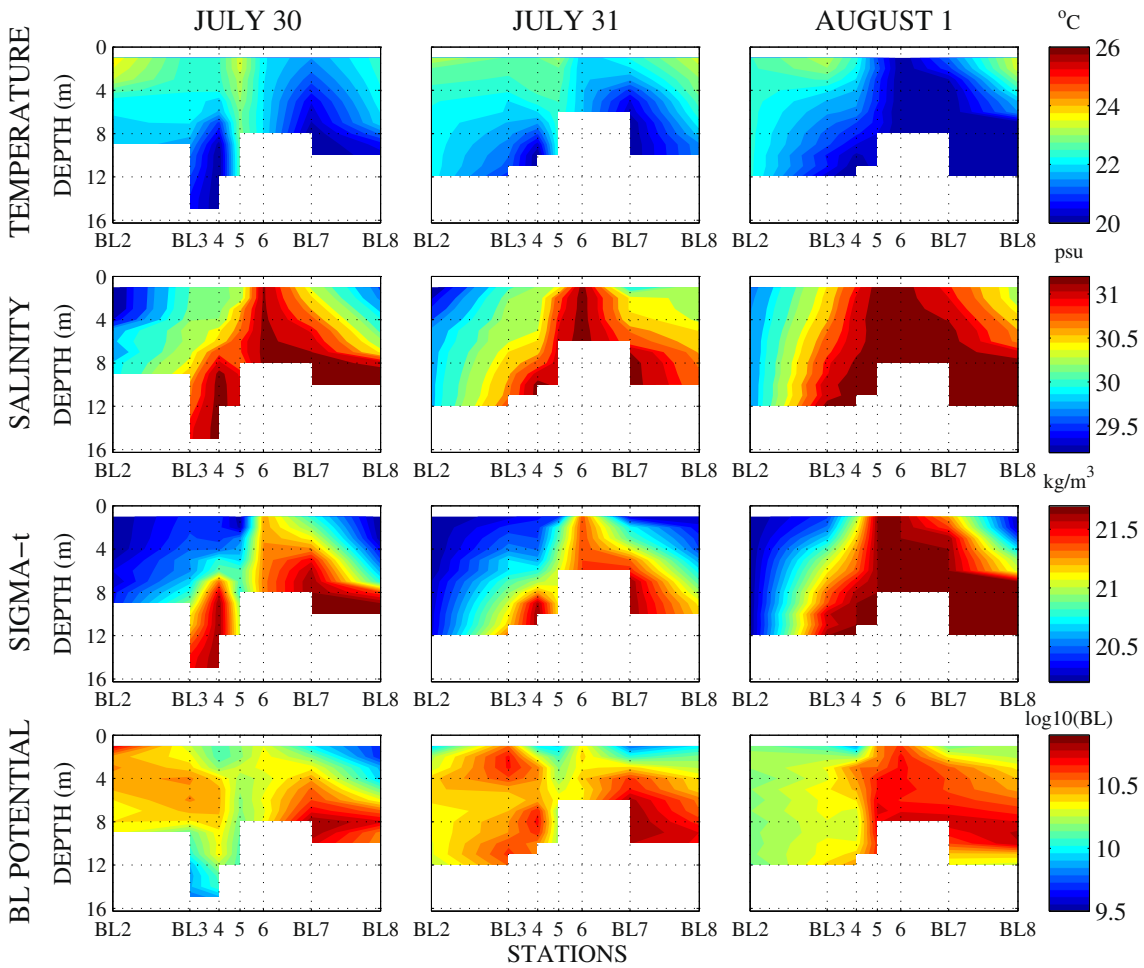

Fig. 7 The observed temperature, salinity, sigma-t, and BL potential along the stations crossing the Bay's mouth

area and facilitate consumption of nutrients (however, we do not have observations supporting this).

There are no available bio-optical, physical observations and mature bio-optical models to quantify the advection versus local processes in the formation of the observed submesoscale filament. For this reason, we compare here the time scales of considered processes.

With the MLD around 10 m and vertical velocities of order 10^{-4} m/s (Figs. 4f and 5), the time scale of ASC cells is around 1.1 days. This time scale is in the ranges of observed time scales of phytoplankton growth rates (Feng et al. 2007) in the Delaware Bay. With spatial scales of 10–40 km, the time scale for horizontal advection by typical surface velocities of order 0.2–0.4 m/s (Fig. 3) is around 0.3–2.4 days. Therefore, ASC cells, horizontal advection, and phytoplankton growth rates have similar time scales during the development of the observed chlorophyll-a filament.

Figure 6 shows the dynamics of the BL potential over 3 days of sampling at stations BL5, BL6, BL7, and BL8. Stations BL5 and BL6 are located at the entrance of the bay, while stations BL7 and BL8 are located offshore in the submesoscale filament (Fig. 4c). During the first two nights of surveys, values of BL potential at stations located in the submesoscale chlorophyll-a filament (stations BL7 and BL8) are lower at 1-m depth but higher at 6- and 11-m depths than at stations located at the entrance of the bay (stations BL5 and BL6). There are increases in BL potential values at the entrance of the bay during the third day (stations BL5 and BL6, night survey of August 1). To better understand the observed increase over 3 days in BL potential values at the entrance of the bay, we analyzed the observed temperature, salinity, sigma-t, and BL potential along the stations crossing the Bay's mouth (Fig. 7). Profiles are binned into 1-m bins (all data from downward and upward profiles were combined together and binned), and then bins are interpolated along the line connecting stations (from BL2 to BL8). Figure 7 shows the presence of a strong frontal structure in the area of station BL6 during surveys of July 30 and 31. This front separates colder, more saline, denser offshore water with elevated BL potential values (stations BL7 and BL8 in the area of submesoscale filament) from the bay water masses. This correlates with the also observed elevated values of BL potential in the

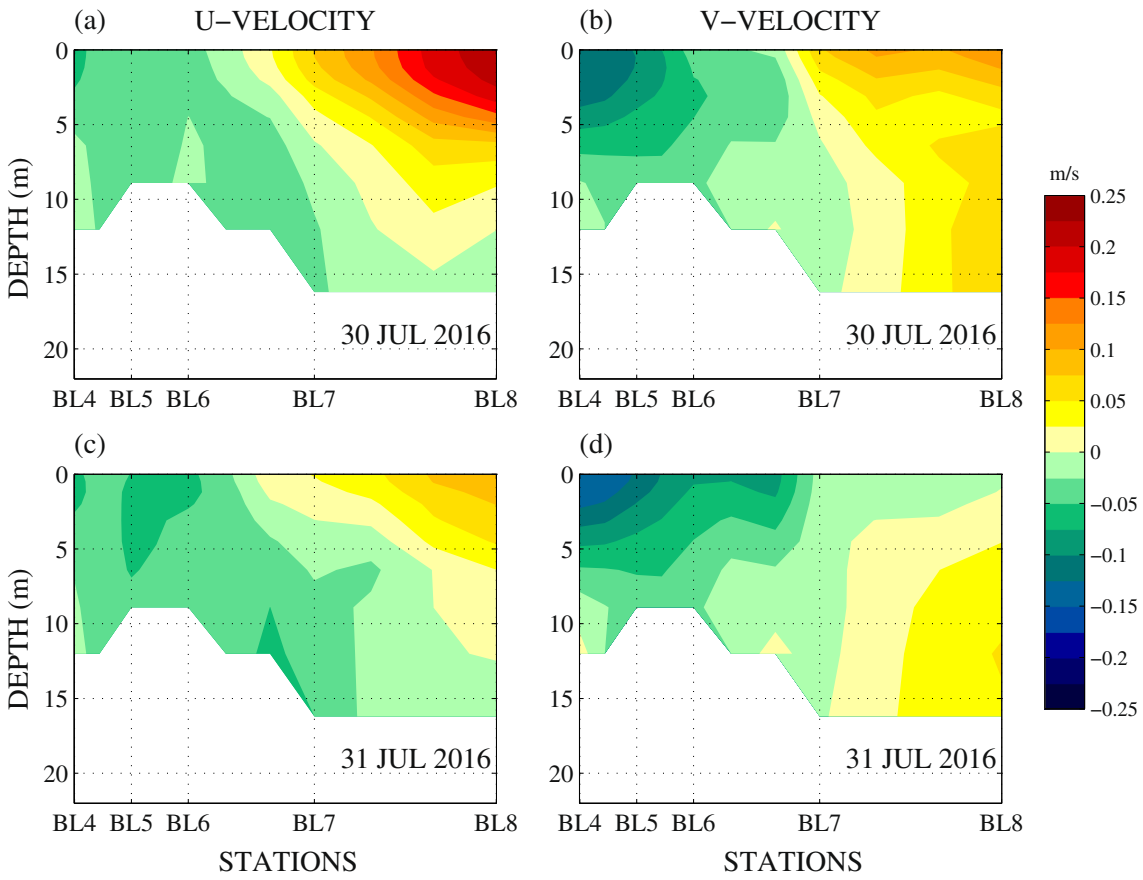

Fig. 8 The FDEL horizontal velocity along the stations BL4 to BL8. **a** Zonal and **b** meridional components of daily averaged subsurface horizontal velocity centered at 12Z of July 30, 2015. **c** Zonal and **d** meridional components of daily averaged subsurface velocity centered at 12Z of July 31, 2015

submesoscale filaments in the Monterey Bay, CA, where the productive filaments incubate bioluminescent plankton population (Shulman et al. 2015). Figure 7 indicates that by August 1, this front and offshore water masses (from stations BL7–BL8) moved to the entrance of the bay toward stations B3–B4. This onshore movement can be explained by the short reversal of winds from upwelling to downwelling favorable during the second half of July 31, as indicated by the Fig. 3a. It is known (e.g., Whitney and Garvine 2006) that upwelling favorable winds (blowing up shelf) drives the offshore Ekman transport, while downwelling favorable wind (blowing down the shelf) drives inshore Ekman transport. Figure 8 shows the daily averaged subsurface horizontal velocities centered at 12Z of July 30 versus the daily averaged subsurface horizontal velocities centered at 12Z of July 31. On July 30 (when upwelling winds dominate), Fig. 8a, b shows a strong offshore and northward flow in the surface, and up to 10-m depth between offshore stations BL7 and BL8 (zonal (U) and meridional (V) components of velocity are positive). Also, there is a very weak inshore flow below 10 m from the offshore stations (BL7 and BL8) toward the entrance to the bay (stations BL5–BL6). In contrast, on July 31 (when short downwelling event was present during second half of July 31), there is a much weaker offshore flow only up to 5-m depth between offshore stations BL7 and BL8. At the same time, there is a much stronger onshore flow below 5-m depth from offshore stations toward stations at the entrance to the bay. This supports the observed inshore translation of offshore water masses toward the entrance of the Bay on Fig. 7. This onshore migration of offshore water brought with it offshore BL plankton communities with higher BL potential. These dynamics of BL potential changes during 3 days of surveys are well supported and illustrated by plots of histograms of BL potential on Fig. 9. For July 30, at stations BL5 and BL6, the BL potential values associated with maxima of flash counts (for 6- and 11-m depths) are lower in comparison to the BL potential values associated with maxima of flash counts for the offshore station BL7. Two days later, on August 1, the BL potential values associated with maxima of flash counts (for 6- and 11-m depths) are aligned and comparable for all three stations. This supports the conclusion that the BL communities which were offshore on July 30 are the source of the increase in BL potential at the entrance of the bay 2 days later. Based on the histogram for BL7, we can speculate that there are two communities of bioluminescent organisms: likely dinoflagellates with lower BL potential at 1 m (Fig. 9) and

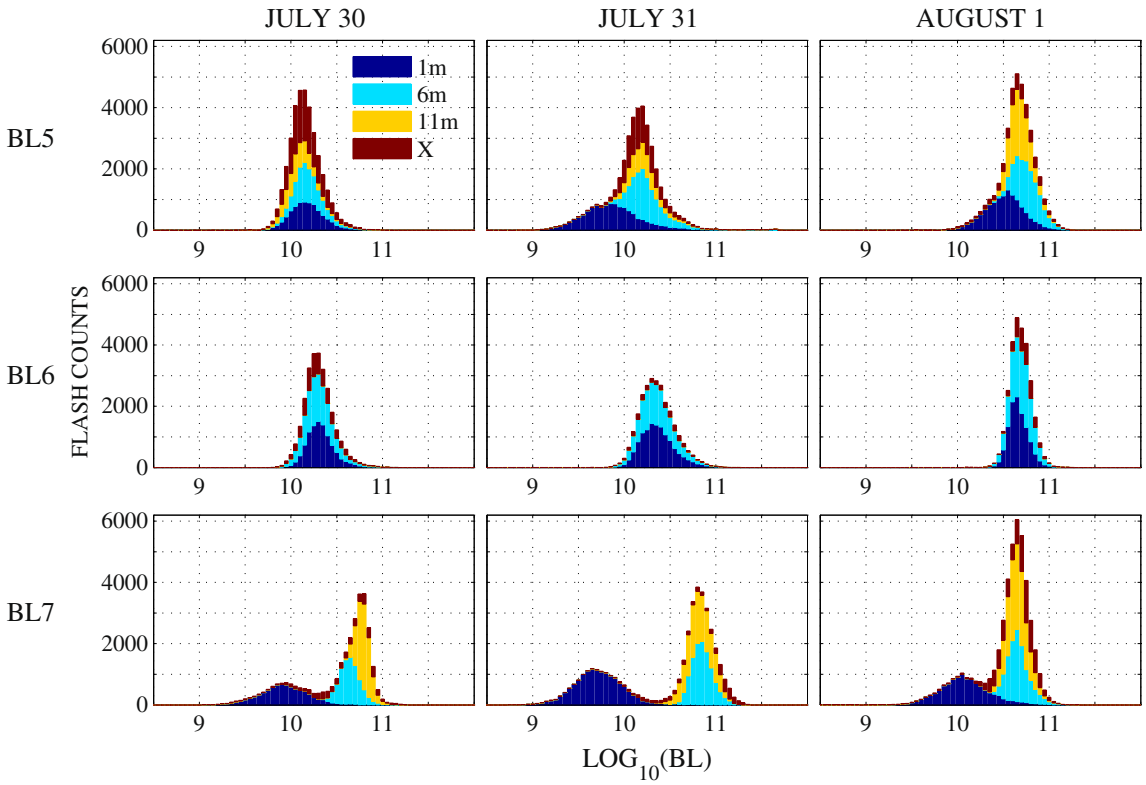

Fig. 9 Histograms of BL potential at different depths at stations BL5, BL6, and BL7 (notation *X* means other than 1-, 6-, or 11-m depths)

zooplankton communities in deeper waters at 6 and 11 m (Fig. 9). This is in agreement with studies to provide fine-scale resolution of populations of zooplankton and dinoflagellates by using BL potential and intensity of flashes (Widder and Johnsen 2000; Moline et al. 2010; Johnsen et al. 2014; Cronin et al. 2016).

The BLP station is located in the area of the Delaware Coastal Current (DCC; Fig. 1), which flows downstream from the mouth of Delaware Bay (Whitney and Garvine 2006) and where upwelling favorable winds reverse the southward flow of DCC and take the buoyant outflow to the north up the shelf. In accord with Fig. 4c, the station BLP is also located at the base of the productive submesoscale filament. The area around the BLP station was sampled again on the night of August 19 (see stations locations on Fig. 1). During the survey, there were weak upwelling favorable winds (Fig. 10), and the HF radar surface currents for August 19 show weaker but similar upwelling circulation patterns observed during the July 30–August 1 surveys of the BLP station (Fig. 3). As during the first survey (Fig. 4c), the satellite VIIRS image for August 17 (Fig. 10c) shows a development of the submesoscale filament with elevated chlorophyll-a content. The chlorophyll-a values in this submesoscale filament on August 17 are lower than in the submesocale filament observed during the first survey (July 31, Fig. 4c). Figure 11 shows a temperature versus salinity diagrams where points are colored with the values of BL potential. For points with the same values of temperature and salinity, values of BL potential are sorted where higher values appear above lower values. There is a distinct separation of the July 30–August 1 survey from the August 19 one. The water masses from the August 19 survey are more salty with the difference in salinity reaching more than 1 ppt for some points with the same temperature. Figure 11 also shows temperature versus salinity diagrams (also colored with the corresponding BL potential values) for different depth bins. It shows that for all depth bins (for the entire water column), the water masses from the August 19 survey have greater salinity than water masses from the July 30–August 1 survey. Figure 10d shows the USGS Delaware River daily discharge record at Trenton, NJ. The record indicates that river discharges before and during the first survey (July 30–August 1) were stronger than before and during the August 19 survey. This explains the presence of the more saline water masses during the August 19 survey. Based on Figs. 11, comparisons of points below 2.5-m depth with the same temperature for both surveys show that for most of them, the maxima of BL potential from the July 30 to August 1 survey are higher than the maxima of BL potential for the August 19 survey. Therefore, the submesoscale filament of July 30–August 1 with lower salinity and higher biomass (Figs. 4c and 10c)

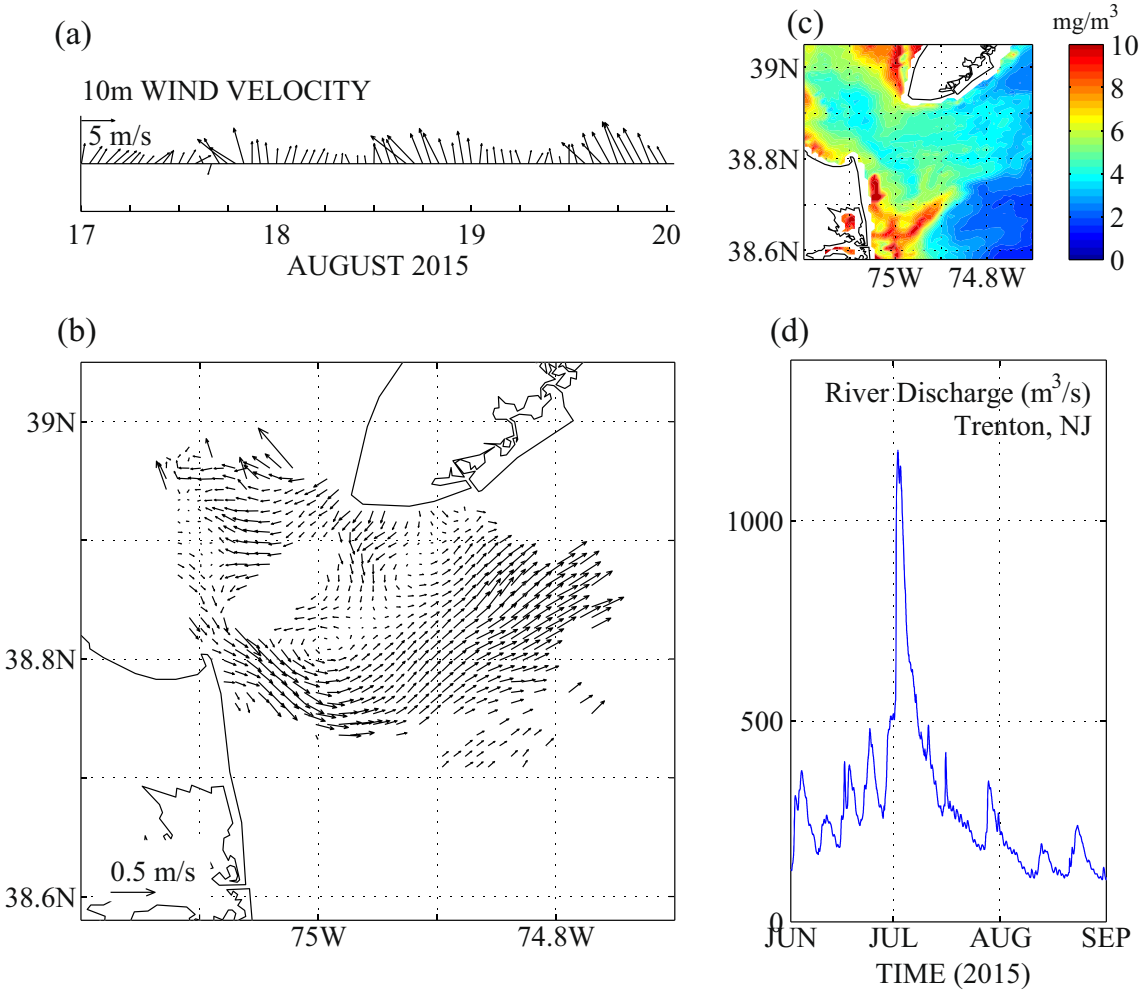

Fig. 10 **a** Ten-meter wind velocity at the NOAA Lewes station during August 17–20 of 2015. **b** 33-h low-passed HF radar surface currents at August 17, 2015. **c** VIIRS image of chlorophyll-a on August 17, 2015. **d** the USGS Delaware River daily discharge record at Trenton, NJ

incubates bioluminescent communities which have higher values of BL potential in comparison to the August 19 filament.

4 Discussions and conclusions

We present the first (to our knowledge) observational and modeling studies of BL potential dynamics in the Delaware Bay area. Analysis of observations and modeling results show typical patterns for upwelling surface circulation during the BL potential sampling. There is a buoyant, less saline water outflow through the south of the Delaware Bay mouth. This outflow is advected offshore and to the north by the northward currents. The satellite VIIRS imagery shows the presence of submesoscale filament with elevated chlorophyll-a content in the area of interaction of the buoyant, less saline outflow with denser upwelled offshore waters. Observations and model results have shown the generation of ageostrophic secondary circulation (ASC) cells in the area of the filament with upwelling on the warm side of the front and downwelling on the cold side. Because the MLD is shallower than the estimated euphotic depth in and around the filament, the developed ASC cells kept phytoplankton in the lighted area and supported photosynthesis. We have shown that during the development of the observed chlorophyll-a filament, time scales of ASC cells, advection, and observed phytoplankton growth rates are comparable in the area. Analysis of BL potential observations has shown elevated values of BL potential in the area of the submesoscale filament, which indicates that productive submesoscale filament incubates the bioluminescent plankton. This is in agreement with our previous findings in the Monterey Bay area, where observations and modeling studies have shown that productive offshore submesoscale filaments also incubate bioluminescent plankton population.

Over 3 days of Bl potential sampling, the onshore (toward the mouth of the Bay) migration of the offshore filament was observed. This onshore move of offshore water masses

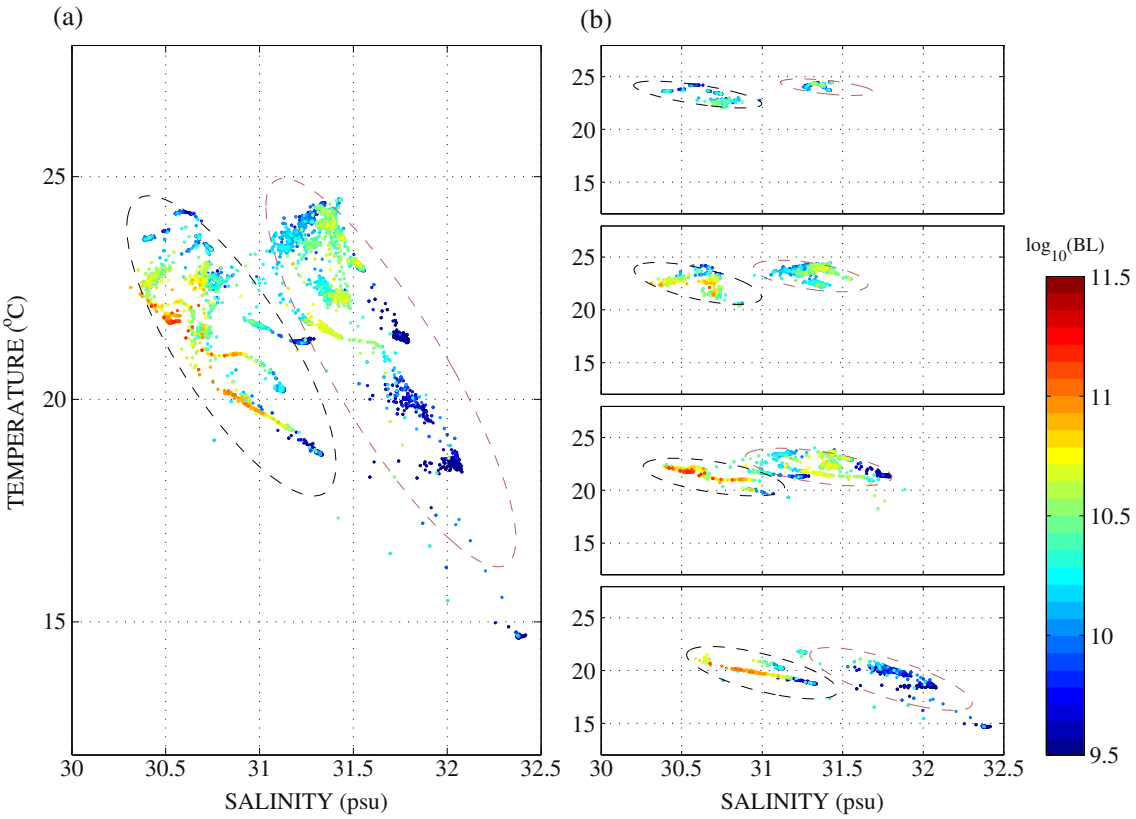

Fig. 11 Observed temperature versus salinity diagrams for **a** whole depths and **b** separately for different depth bins. Points are colored with the values of BL potential. Cloud of points inside *black dashed ellipses* belong to July 30–August 1 survey, while cloud of point inside of *brown dashed ellipses* are belong to August 19 survey

brought offshore BL plankton communities with higher values of BL potential. We have shown that this onshore translation of the offshore frontal structure is a result of a short wind reversal event (from upwelling to downwelling) during the second day of sampling, when the offshore Ekman transport by the upwelling favorable winds weakened and reversed to the inshore transport.

We have compared two surveys (at the end of July and in the middle of August) of water masses located in the area where the buoyant outflow of the Delaware Coastal Current is turned around and taken to the north up the shelf by upwelling favorable winds. As indicated by satellite imagery, during both surveys, the sampling areas are located at the bases of the submesoscale productive filaments extending from the coast to the north along the shelf. Observations show that the submesoscale filament of July 30–August 1 has fresher water masses (result of higher river runoff before and during survey), higher chlorophyll-a content, and incubates bioluminescent communities with higher values of BL potential in comparison to the submesoscale filament in the middle of August.

In the present study of the Delaware Bay area, we have shown that BL potential dynamics are impacted by the submesoscale processes due to the interaction between buoyant river outflow with cold and saline upwelled water. Our previous observational and modeling studies in Monterey Bay have shown that processes such as upwelling/downwelling, coastally trapped waves (CTW), submesoscale processes, phytoplankton blooms and plankton migration impact dynamics, and changes in BL potential. As a result, the sustained presence in the area on time scales of weeks to months, and with sampling extended to 1000 km, are needed in order to resolve BL potential dynamics. With this in mind, sampling is also needed with very high spatial resolution, because observed de-correlation scales of BL potential can range from 0.8 to 7 km (Moline et al. 2010). Bioluminescence potential sensors are now integrated into ship and propeller-driven unmanned underwater vehicles (UUVs) surveys and into profilers on moorings (Haddock et al. 2010; Moline et al. 2014). Ship surveys and propeller-driven UUVs provide synoptic sampling of BL potential. However, those platforms cannot provide a sustained presence in the area and sampling on needed temporal and spatial scales. Gliders have proven their ability to sample oceanic properties with high spatial resolution, and on time scales of weeks to months and with spatial coverage extending to 1000 km. Also, with slow-moving gliders with a BL sensor on board, there is potential for a better account of the variability in organisms' abundance and improved resolution of the

variability in the BL potential. The development and testing of new technology using gliders with BL potential sensors is needed and this will require research and development of new paradigms for the BL potential sampling, mapping and modeling.

Acknowledgements This research was funded through the US Naval Research Laboratory under program element 61153N and grants N0001415WX01395, N0001416WX01092, N00014-14-1-0841, and N00015-15-1-2624 sponsored by the Office of Naval Research, Littoral Geosciences and Optics program. We thank Adam Lawson for help with processing satellite imagery, and we thank Brent Bartels of QinetiQ North America for help with the computer code estimating Q vector. We thanks Hunter C. Brown, Danielle Haulsee, Matt Breece, Megan Cimino, and Jason Moline for assistance in measurements and Kevin Beam for captaining the R/V Daiber. We thank anonymous reviewers for providing very insightful comments and recommendations to improve the paper. Computer time for the numerical simulations was provided through a grant from the Department of Defense High Performance Computing Initiative. Request for access to the data presented in this paper can be sent to igor.shulman@nrlssc.navy.mil. This manuscript is US NRL contribution 7330-16-3187.

References

Arnone R, Fargion G, Martinolich P et al. (2012) "Validation of the VIIRS ocean color", Proc. SPIE 8372, Ocean sensing and monitoring IV, 83720G, doi:10.1117/12.922949

Calil PHR, Richards KJ (2010) Transient upwelling hot spots in the oligotrophic North Pacific. J Geophys Res 115:C02003. doi:10.1029/2009JC005360

Chassignet EP, Hurlburt HE, Metzger EJ, Smedstad OM, Cummings J, Halliwell GR, Bleck R, Baraille R, Wallcraft AJ, Lozano C, Tolman HL, Srinivasan A, Hankin S, Cornillon P, Weisberg R, Barth A, He R, Werner F, Wilkin J (2009) U.S. GODAE: global ocean prediction with the HYbrid Coordinate Ocean model (HYCOM). Oceanography 22(2):64–75

Cronin HA, Cohen JH, Berge J, Johnsen G, Moline MA (2016) Bioluminescence as an ecological factor during high Arctic polar night. Sci Rep 6:36374. doi:10.1038/srep36374

Cummings JA (2005) Operational multivariate ocean data assimilation. Q J R Meteorol Soc 131:3583–3604. doi:10.1256/qj.05.105

Egbert GD, Erofeeva SY (2002) Efficient inverse modeling of barotropic ocean tides. J Atmos Ocean Technol 19:183–204

Feng Y, Zhang Y, Hutchins DA (2007) Fast microzooplankton grazing on fast-growing, low-biomass phytoplankton: a case study in spring in Chesapeake Bay, Delaware inland bays and Delaware Bay. Hydrobiologia 589:127–139. doi:10.1007/s10750-007-0730-6

Flather RA (1976) A tidal model of the northwest European continental shelf. Memorie Societa Real Scienze Liege 6:141–164

Fong DA, Geyer WR (2001) The response of a river plume during an upwelling favorable event. J Geophys Res 106:1055–1062

Haddock SHD, Moline MA, Case JF (2010) Bioluminescence in the sea. Annu Rev Mar Sci 2:443–493

Herren CM, Haddock SHD, Johnson C, Orrico CM, Moline MA, Case JF (2005) A multi-platform bathyphotometer for fine-scale, coastal bioluminescence research. Limnol Oceanogr Methods 3:247–262

Hoskins BJ (1982) The mathematical theory of frontogenesis. Annu Rev Fluid Mech 14:131–151. doi:10.1146/annurev.fl.14.010182.001023

Houghton RW, Tilburg CE, Garvine RW, Fong A (2004) Delaware River plume response to a strong upwelling-favorable wind event. Geophys Res Lett 31:L07302. doi:10.1029/2003GL018988

Hu C, Lee Z, Franz BA (2012) Chlorophyll-a algorithms for oligotrophic oceans: a novel approach based on three-band reflectance difference. J Geophys Res 117:C01011. doi:10.1029/2011JC007395

Joesoef A, Huang W-J, Gao Y, Cai W-J (2015) Air–water fluxes and sources of carbon dioxide in the Delaware estuary: spatial and seasonal variability. Biogeosciences 12:6085–6101. doi:10.5194/bg-12-6085-2015

Johnsen G, Candeloro M, Berge J, Moline MA (2014) Glowing in the dark: discriminating patterns of bioluminescence from different taxa during the Arctic polar night. Polar Biol 37:707–713

Kara AB, Rochford PA, Hurlburt HE (2003) Mixed layer depth variability over the global ocean. J Geophys Res 108(C3):3079. doi:10.1029/2000JC000736

Kundu PK (1976) Ekman veering observed near the ocean bottom. J Phys Oceanogr 6:238–242

Ladner S, Arnone R, Martinolich P et al. (2014) Inter-satellite comparison and evaluation of navy SNPP-VIIRS and MODIS aqua ocean color properties. Proc. SPIE 9111, Ocean Sensing and Monitoring VI, 911107. doi:10.1117/12.2053060

Lee ZP, Darecki M, Carder KL, Davis CO, Stramski D, Rhea WJ (2005) Diffuse attenuation coefficient of downwelling irradiance: an evaluation of remote sensing methods. J Geophys Res 110:C02017. doi:10.1029/2004JC002573

Lee ZP, Weidemann A, Kindle J, Arnone R, Carder KL, Davis C (2007) Euphotic zone depth: its derivation and implication to ocean color remote sensing. J Geophys Res 112:C03009. doi:10.1029/2006JC003802

Levy M, Ferrari R, Franks PJS, Martin AP, Rivière P (2012) Bringing physics to life at the submesoscale. Geophys Res Lett 39:L14602. doi:10.1029/2012GL052756

Marcinko CLJ, Painter SC, Martin AP, Allen JT (2013) A review of the measurement and modelling of dinoflagellate bioluminescence. Prog Oceanogr 109:117–129

Marcinko CLJ, Martin AP, Allen JT (2014) Modelling dinoflagellates as an approach to the seasonal forecasting of bioluminescence in the North Atlantic. J Mar Syst 139:261–276. doi:10.1016/j.jmarsys.2014.06.014

Metzger EJ, Smedstad OM, Thoppil PG, Hurlburt HE, Cummings JA, Wallcraft AJ, Zamudio L, Franklin DS, Posey PG, Phelps MW, Hogan PJ, Bub FL, DeHaan CJ (2014) US navy operational global ocean and Arctic ice prediction systems. Oceanography 27(3):32–43 http://dx.doi.org/10.5670/oceanog.2014.66

Moline MA, Blackwell SM, Allen B, Austin T, Forrester N, Goldsborogh R, Purcell M, Stokey R, von Alt C (2005) Remote environmental monitoring units: an autonomous vehicle for characterizing coastal environments. J Atmos Ocean Technol 22:1798–1809

Moline MA, Blackwell SM, Case JF, Haddock SHD, Herren CM, Orrico CM, Terrill E (2009) Bioluminescence to reveal structure and interaction of coastal planktonic communities. Deep-Sea Res 56:232–245. doi:10.1016/j.dsr2.2008.08.002

Moline MA, Benoit-Bird KJ, Robbins IC, Schroth-Miller M, Waluk CM, Zelenke B (2010) Integrated measurements of acoustical and optical thin layers II: horizontal length scales. Cont Shelf Res 30:29–38. doi:10.1016/j.csr.2009.08.004

Moline, M. A., M. Oliver, C. Orrico, R. Zaneveld, I. Shulman (2013) Bioluminescence in the sea. Book Chapter 7. Subsea Optics and Imaging, Woodhead Publishing, 134–170. doi:10.1533/9780857093523.2.134

Muscarella PA, Barton NP, Lipphardt BL Jr, Veron DE, Wong K-C, Kirwan AD Jr (2011) Surface currents and winds at the Delaware Bay mouth. Cont Shelf Res 31:1282–1293

Ondercin DG, Atkinson CA, Kiefer DA (1995) The distribution of bioluminescence and chlorophyll during the late summer in the North-Atlantic—maps and a predictive model. J Geophys Res Oceans 100: 6575–6590

Pennock JR, Sharp JH (1986) Phytoplankton production in the Delaware estuary: temporal and spatial variability. Mar Ecol Prog Ser 34:143–155

Pollard RT, Regier LA (1992) Vorticity and vertical circulation at an ocean front. J Phys Oceanogr 22(6):609–625

Rudnick DL (1996) Intensive surveys of the Azores front. Part II: inferring the geostrophic and vertical velocity fields. J Geophys Res 101: 16291–16303

Sanders TM, Garvine RW (2001) Fresh water delivery to the continental shelf and subsequent mixing: an observational study. J Geophys Res 106(C11):27087–27101

Shulman I, Anderson S, Rowley C, deRada S, Doyle J, Ramp S (2010) Comparisons of upwelling and relaxation events in the Monterey Bay area. J Geophys Res 115:C06016. doi:10.1029/2009JC005483

Shulman I, Moline MA, Penta B, Anderson S, Oliver M, Haddock SHD (2011) Observed and modeled bio-optical, bioluminescent, and physical properties during a coastal upwelling event in Monterey Bay, California. J Geophys Res 116:C01018. doi:10.1029/2010JC006525

Shulman I, Penta B, Moline MA, Haddock SHD, Anderson S, Oliver M, Sakalaukus P (2012) Can vertical migrations of dinoflagellates explain observed bioluminescence patterns during an upwelling event? J Geophys Res 117:C01016. doi:10.1029/2011JC007480

Shulman I, Penta B, Richman J et al. (2015) Impact of submesoscale processes on dynamics of phytoplankton filaments, J Geophys Res Oceans, 120, doi:10.1002/2014JC010326

Wang Z, Haidvogel D, Bushek D, Ford S, Hofmann EE, Powell EN, Wilkin J (2012) Circulation and water properties and their relationship to the oyster disease MSX in Delaware Bay. J Mar Res 70:279–308

Whitney MM, Garvine RW (2005) Wind influence on a coastal buoyant outflow. J Geophys Res 110:C03014. doi:10.1029/2003JC002261

Whitney MM, Garvine RW (2006) Simulating the Delaware buoyant outflow: comparison to observations. J Phys Oceanogr 36:3–21

Widder EA (2010) Bioluminescence in the ocean: origins of biological, chemical and ecological diversity. Science 328:704

Widder EA, Johnsen S (2000) 3D spatial patterns of bioluminescent plankton: a map of the "minefield". J Plankton Res 22:409–420

Wilks DS (1995) Statistical methods in the atmospheric sciences, 467 pp. Academic, San Diego